Fourier transform microwave spectrum of difluoromethane–Xe

ARTICLE *in* JOURNAL OF MOLECULAR SPECTROSCOPY · NOVEMBER 2009

Impact Factor: 1.48 · DOI: 10.1016/j.jms.2009.09.006

3 AUTHORS, INCLUDING:

Shouyuan Tang
Chongqing University
11 PUBLICATIONS **57** CITATIONS

SEE PROFILE

Journal of Molecular Spectroscopy 258 (2009) 71–74

Contents lists available at ScienceDirect

Journal of Molecular Spectroscopy

journal homepage: www.elsevier.com/locate/jms

Fourier transform microwave spectrum of difluoromethane–Xe

Shouyuan Tang [1], Luca Evangelisti, Walther Caminati *

Dipartimento di Chimica "G. Ciamician", dell'Università, Via Selmi 2, I-40126 Bologna, Italy

ARTICLE INFO

Article history:
Received 17 July 2009
In revised form 16 September 2009
Available online 24 September 2009

Keywords:
Rotational spectroscopy
Molecular complexes
Large amplitude motions
Quadrupole coupling: pulsed jets
Xenon

ABSTRACT

The microwave spectra of three isotopomers of the complex of difluoromethane–xenon (^{132}Xe, ^{131}Xe, ^{129}Xe) have been studied by supersonic jet Fourier transform microwave spectroscopy. A general improvement of the fittings has been obtained with respect to a previous millimeter wave free jet investigation (Caminati, 2006) [12]. In particular, the nuclear quadrupole coupling constants of the ^{131}Xe nucleus in difluoromethane–^{131}Xe have been precisely determined, χ_{aa} = 0.941(4), χ_{bb} = 0.642(4) and χ_{cc} = −1.583(4) MHz, respectively.

1. Introduction

Isolated rare gas (RG) atoms have an isotropic electron distribution, which correspond to a zero value of the electric field gradient, $q_{gg} = (\partial^2 V/\partial g^2)_0$, $g = x, y, z$, at the nucleus. Such an isotropy is slightly distorted when the rare gas atom interacts with the nuclear and electronic charges of a partner molecule in a molecular complex. If we take into account an isotopic species of a rare gas atom with a nuclear spin $I \geqslant 1$, a coupling between the overall rotation and the nuclear spin takes place and the corresponding quadrupole coupling constants χ_{gg} can be determined. It is then possible to obtain the field gradient from the relation $\chi_{gg} = eQq_{gg}$, where e is the electron electrical charge and Q the nuclear electric quadrupole moment. Among the rare gas atoms, ^{21}Ne (0.26%, 3/2, 0.09), ^{83}Kr (11.6%, 9/2, 0.23) and ^{131}Xe (21.2%, 3/2, −0.12)—in parenthesis the natural abundance, I and Q—are the only isotopes which possess this property.

The ^{21}Ne, ^{83}Kr and ^{131}Xe χ quadrupole coupling constants have been determined so far—to our knowledge—for 1, 2 and 3 RG–RG′ complexes, respectively. The obtained values are $\chi(^{21}\text{Ne})$ = −30(2) kHz in ^{21}Ne–^{40}Ar [1], $\chi(^{83}\text{Kr})$ = −0.5205(23) and −0.8529(14) MHz in ^{20}Ne–^{83}Kr and ^{40}Ar–^{83}Kr, respectively [2], and $\chi(^{121}\text{Xe})$ = 0.3878(9), 0.7228(36), 0.7079(86) MHz in ^{20}Ne–^{131}Xe, ^{40}Ar–^{131}Xe and ^{84}Kr–^{131}Xe, respectively [3]. One can note that: (i) the quadrupole coupling constant is related to the polarizability of the atom of interest; (ii) the sign is different for Ne, Kr compared to Xe, according to the sign of Q.

The natural abundance of ^{131}Xe is considerably higher than those of the two related RG nuclei; probably for this reason the quadrupole coupling tensor has been determined also for several asymmetric top RG-molecule complexes [4–9].

Recently we investigated the millimeter wave spectra of some complexes of difluoromethane (DFM) with rare gases [10–12]. A tunnelling splitting (ΔE) was observed, being of 193.5, 79.19 and 39.1 MHz for DFM–Ar [10], DFM–Kr [11] and DFM–Xe [12], respectively. Such a splitting was used to determine the potential energy surface of the RG motions with respect to DFM. In the case of DFM–Xe, the mmw rotational spectrum has been reported for the DFM–^{129}Xe, DFM–^{132}Xe and DFM–^{131}Xe isotopologues. In all cases, the value of the ΔE splitting was not precisely determined because the Coriolis coupling constants, the centrifugal distortion constants and ΔE itself were strongly correlated to each other. The mmw spectrum of the DFM–^{131}Xe isotopologues was much weaker than expected from the relative isotopic abundance, due to the broadening of the transitions by the ^{131}Xe quadrupolar effects. In order to improve the fitting and also to determine the ^{131}Xe quadrupole tensor also for this complex, we decided to investigate its pulsed jet Fourier transform microwave (FTMW) spectrum, that is with a technique with a much higher resolving power.

2. Experimental

DFM and xenon (99.997%) have been supplied by Linde and Rivoira, respectively, and used without further purification. The pulsed jet Fourier transform microwave [13] spectrometer was described elsewhere [7], and recently updated with the FTMW++ set

* Corresponding author. Fax: +39 051 2099456.
E-mail address: walther.caminati@unibo.it (W. Caminati).
[1] Present address: College of Bioengineering, ChongQing University, ChongQing 400044, PR China.

0022-2852/$ - see front matter © 2009 Elsevier Inc. All rights reserved.
doi:10.1016/j.jms.2009.09.006

of programs [14]. For the production of the complex, a 2% mixture of DFM in xenon at a backing pressure of 2 bar was flown through the solenoid valve (General Valve, Series 9) and expanded into the cavity, to about 10^{-5} mbar. Each rotational transition is split by the Doppler effect, enhanced by the coaxial expansion of the supersonic jet with the resonator axis. The rest frequency is the arithmetic mean of the frequencies of the two Doppler components. The estimated accuracy of the frequency measurements is less than 3 kHz and lines separated by more than 7 kHz are resolvable.

3. Rotational spectra and analysis

The geometry of the xenon atom in the molecular complex is shown in Fig. 1. From the rotational constants obtained by millimeter wave absorption spectroscopy [12], it was easy to locate the rotational transitions of the DFM–^{132}Xe and DFM–^{129}Xe species in the lower frequency range of our pulsed jet Fourier transform microwave spectrometer. 10 μ_c-type transitions and 18 μ_a-type transitions have been measured for DFM–^{132}Xe and DFM–^{129}Xe, respectively. All transitions were split into two component lines, due to the tunneling motion of xenon atom with respect to DFM. The measured line frequencies are listed in Table 1. They have been fitted, together with the frequencies of the previously measured millimeter transitions, to obtain the spectroscopic constants reported in the first two columns of data of Table 2. A Pickett-type coupled Hamiltonian has been used for fitting, in the form of SPFIT program [15], according to:

$$H = H_R(0^+) + H_R(0^-) + H_{CD} + \Delta E \quad (1)$$

$H_R(0^+)$ and $H_R(0^-)$ represent the rigid rotational parts of Hamiltonian for the 0^+ and 0^- states, respectively. H_{CD} gives the centrifugal distortion contribution (S-reduction and I^r-representation) [16], which is assumed to be the same in both states. ΔE is the vibrational spacing between the two states.

It was then possible to analyze the spectrum of the DFM–^{131}Xe isotopologue and obtain the nuclear quadrupole coupling constants. Again 7 μ_c-type transitions were measured. Each of them was further split due to the nuclear spin. The rotational transition patterns were rather complicated due to the numerous quadrupole and tunneling component lines. The two tunneling component lines of the $4_{1,3} \leftarrow 3_{0,3}$ transition are shown in Fig. 2 for the DFM–^{131}Xe (top, with the quadrupole hyperfine structure) and DFM–^{132}Xe (bottom) species. One can see the splittings due to tunneling motion and ^{131}Xe nuclear coupling (a and b). The two pairs of equivalent fermions (H–H and F–F) produce a 10/6 statistical weight, observed for all lines. It depends on the parities of K_a and

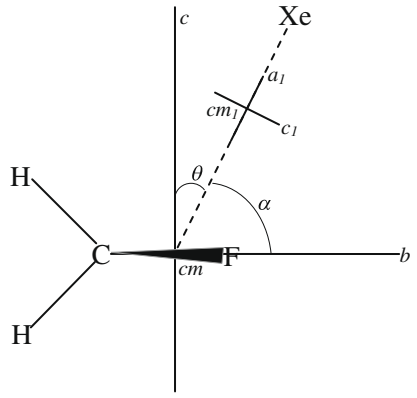

Fig. 1. Sketch of DFM–Xe, together with the principal axes systems of DFM and of DFM–Xe, and the van der Waals structural parameters used in the text.

Table 1
Experimental transition frequencies [$J'(K_a',K_c') \leftarrow J''(K_a'',K_c'')$, MHz] of DFM–^{129}Xe, DFM–^{132}Xe and DFM–^{131}Xe.

μ_c Transitions	DFM–^{129}Xe		DFM–^{132}Xe		μ_c Transitions	DFM–^{131}Xe		
	$0^- \leftarrow 0^+$	$0^+ \leftarrow 0^-$	$0^- \leftarrow 0^+$	$0^+ \leftarrow 0^-$		$F' \leftarrow F''$	$0^- \leftarrow 0^+$	$0^+ \leftarrow 0^-$
1(1,1) ← 1(0,1)	8679.4967	8600.9231	8685.1727	8606.7240	1(1,1) ← 1(0,1)	5/2–5/2	8683.3263	8604.8242
1(1,0) ← 0(0,0)	10518.3817	10439.8156	10512.3391	10433.8903		3/2–3/2	8683.2483	8604.7524
2(1,1) ← 1(0,1)	12356.6901	12278.2142	12338.9316	12260.5809		1/2–1/2	8683.3792	8604.8514
2(1,2) ← 2(0,2)	8617.0340	8538.5105	8623.4691	8545.0733	1(1,0) ← 0(0,0)	5/2–3/2	10514.3930	10435.9090
3(1,3) ← 3(0,3)	8523.9879	8445.5321	8531.5529	8453.2204		3/2–3/2	10513.9974	10435.5177
4(1,4) ← 4(0,4)	8401.1358	8322.7765	8410.1728	8331.9332		1/2–3/2	10514.7077	10436.2277
4(1,3) ← 3(0,3)	16126.1715	16048.0415	16083.8461	16005.8295	2(1,1) ← 1(0,1)	7/2–5/2	12344.8505	12266.4557
5(1,5) ← 5(0,5)	8249.5077	8171.2591	8260.3358	8182.2101		5/2–3/2	12344.4554	12266.0623
5(1,4) ← 4(0,4)	18058.2108	17980.3309	18002.9985	17925.2320		3/2–1/2	12344.9912	12266.6009
6(1,6) ← 6(0,6)	8070.3907	7992.2773	8083.3018	8005.3073		5/2–5/2	12344.6851	12266.2936
μ_a Transitions	$0^+ \leftarrow 0^+$	$0^- \leftarrow 0^-$	$0^+ \leftarrow 0^+$	$0^- \leftarrow 0^-$		3/2–3/2	12344.5628	12266.1742
4(0,4) ← 3(0,3)	7101.9958	7101.9194	7058.2705	7058.1958		1/2–1/2	12345.1532	12266.7599
4(1,3) ← 3(1,2)	7228.4480	7228.3088			2(1,2) ← 2(0,2)	7/2–7/2	8621.3126	
5(0,5) ← 4(0,4)	8874.3097	8874.2161	8819.7245	8819.6328		5/2–5/2	8621.4725	
5(1,5) ← 4(1,4)	8722.7016	8722.6797	8669.9082	8669.8870		3/2–3/2	8621.3454	
5(1,4) ← 4(1,3)	9034.2094	9034.0351	8977.5979	8977.4269		5/2–3/2	8621.6408	
5(2,4) ← 4(2,3)	8875.9072	8875.8090				3/2–1/2	8621.5993	
6(0,6) ← 5(0,5)	10644.5059	10644.3966	10579.1066	10578.9990		5/2–7/2	8621.7004	
6(1,6) ← 5(1,5)	10465.4164	10465.3894	10402.0964	10402.0723	4(1,4) ← 4(0,4)	11/2–11/2	8407.1238	8328.8445
6(1,5) ← 5(1,4)	10839.0640	10838.8558	10771.1652	10770.9600		9/2–9/2	8407.3606	8329.0794
6(2,5) ← 5(2,4)	10649.4982	10649.3865	10583.9088	10583.7947		7/2–7/2	8407.2765	8328.9970
6(2,4) ← 5(2,3)	10661.1372	10661.0102	10595.2566	10595.1342		5/2–5/2	8407.0410	8328.7650
7(0,7) ← 6(0,6)	12412.1689	12412.0476	12336.0118	12335.8917	4(1,3) ← 3(0,3)	11/2–9/2	16097.8377	16019.7879
7(1,7) ← 6(1,6)	12207.1433	12207.1156	12133.3161	12133.2892		9/2–7/2	16097.5209	16019.4683
7(1,6) ← 6(1,5)	12642.8243	12642.5820	12563.6576	12563.4202		7/2–5/2	16097.6558	16019.6080
7(2,6) ← 6(2,5)	12422.2201	12422.0859	12345.7359	12345.6044		5/2–3/2	16097.9742	16019.9248
7(2,5) ← 6(2,4)	12440.8203	12440.6684	12363.8718	12363.7227	5(1,4) ← 4(0,4)	13/2–11/2	18021.2199	17943.4163
9(0,9) ← 8(0,8)	15938.2789	15938.1377	15840.8063	15840.6657		11/2–9/2	18020.9134	17943.1089
9(1,9) ← 8(1,8)	15687.0190	15686.9886	15592.2430	15592.2107		9/2–7/2	18021.0150	17943.2088
9(1,8) ← 8(1,7)			16144.6795	16144.3715		7/2–5/2	18021.3212	17943.5191
10(1,10) ← 9(1,9)			17319.6465	17319.6131	μ_a Transitions		$0^+ \leftarrow 0^+$	$0^- \leftarrow 0^-$
					5(0,5) ← 4(0,4)	Overlapped[a]	8837.6254	8837.5342

[a] Quadrupole component lines overlapped to each other.

Table 2
Spectroscopic parameters of DFM–Xe from the fit of observed experimental frequencies.

	DFM–^{132}Xe	DFM–^{129}Xe	DFM–^{131}Xe
$A(0^+)$/MHz	9559.7882(14)[a]	9559.9123(14)	9559.8255(14)
$B(0^+)$/MHz	913.6062(1)	919.4659(2)	915.5281(6)
$C(0^+)$/MHz	852.0166(2)	857.1114(2)	853.683(3)
$A(0^-)$/MHz	9559.6207(14)	9559.7441(14)	9559.6588(14)
$B(0^-)$/MHz	913.5814(1)	919.4407(2)	915.5031(6)
$C(0^-)$/MHz	852.0218(2)	857.1168(2)	853.689(3)
D_J/kHz	3.678(1)	3.718(1)	3.66(3)
D_{JK}/kHz	108.38(6)	109.71(6)	108.4(1)
D_K/kHz	48.29(16)	49.49(16)	47.3(2)
d_1/kHz	0.237(1)	0.240(1)	0.28(2)
d_2/kHz	0.063(1)	0.065(1)	0.061(4)
H_{JJK}	0.0081(6)	0.0086(6)	0.011(2)
ΔE/MHz	39.316(1)	39.379(1)	39.337(1)
χ_{aa}/MHz			0.941(4)
$(\chi_{bb}-\chi_{cc})$/MHz			2.224(4)
N[b]	80	81	78
σ/σ_{exp}[c]	0.85	0.78	0.62

[a] Errors in parenthesis are expressed in unit of the last digit.
[b] Number of transitions in the fit.
[c] Reduced deviation of the fit when setting the mmw and FTMW measurement errors to 100 and 3 kHz, respectively.

v, and it was discussed in our previous work [12]. The DFM–^{131}Xe measured line frequencies are listed in the right part of Table 1. They have been fitted with the Hamiltonian:

$$H = H_R(0^+) + H_R(0^-) + H_{CD} + H_Q + \Delta E \quad (2)$$

H_Q is nuclear quadrupole coupling with the overall rotation. The H_Q contributions were evaluated in this case according to the coupled basis set $F = J + I_{Xe(131)}$. The obtained spectroscopic parameters are reported in the third column of data of Table 2. The $eQq(^{131}Xe)$ off-diagonal components are not given because not determinable from the fitting of the small splittings.

4. Discussion and conclusions

4.1. Improvement of the fit with respect to the previous study

The number of determined parameters increased from 9 to 13 for the DFM–^{129}Xe and DFM–^{132}Xe species and to 15 for the DFM–^{131}Xe one. The new determined parameters are the centrifugal distortion parameters D_K, d_1, d_2 and H_{JJK}, plus χ_{aa} and $(\chi_{bb}-\chi_{cc})$ for DFM–^{131}Xe. In addition, the uncertainties on the previously reported 9 parameters improved by at least one order of magnitude. Also, the coupling between the centrifugal distortion, the Coriolis coupling parameters and (ΔE) is now almost negligible. The Coriolis coupling parameters were fixed to zero because very small and undetermined from the fit.

Table 3
Quadrupole coupling constants of some Organic Molecule–^{131}Xe molecular complexes.

	Dimethylether–Xe	Pyridine–Xe	CH_2ClF–Xe	DFM–Xe
χ_{aa} (MHz)	4.57(3)	2.735(3)	0.600(7)	0.941(4)
χ_{bb} (MHz)	−2.93(4)	−0.660(2)	0.898(7)	0.642(4)
χ_{cc} (MHz)	−1.64(4)	−2.075(2)	−1.498(7)	−1.583(4)
Reference	[7]	[9]	[8]	This work

4.2. Quadrupole coupling constants

The quadrupole coupling constants are related to the values of the electric field gradients, q_{gg} (g = a, b, c), which are produced by the nuclear and electronic charges of the molecule. We compare in Table 3 the DFM–^{131}Xe quadrupole coupling constants to those so far reported for molecular complexes of xenon with organic molecules. One can see that the χ_{gg} constants of DFM–^{131}Xe are quite similar to those of CH_2ClF–^{131}Xe, in agreement with the fact that CH_2ClF and CH_2F_2 have almost equivalent systems of electrical charges. On the contrary, the complexes of ^{131}Xe with quite different molecules, such as pyridine and dimethylether, generate very different sets of quadrupole coupling constants.

4.3. Tunneling splitting and van der Waals motions

The tunneling splittings obtained in the present work, 39.316, 39.379 and 39.336 MHz for DFM–^{132}Xe, DFM–^{131}Xe and DFM–^{129}Xe, respectively, are quite similar to the previously determined one, and then in agreement with tunneling barrier value of 1.31 kJ/mol given in our previous work [12]. Vice versa, the value of the spectroscopic constant D_J has been reduced from 4.29 to 3.68 kHz with the new,

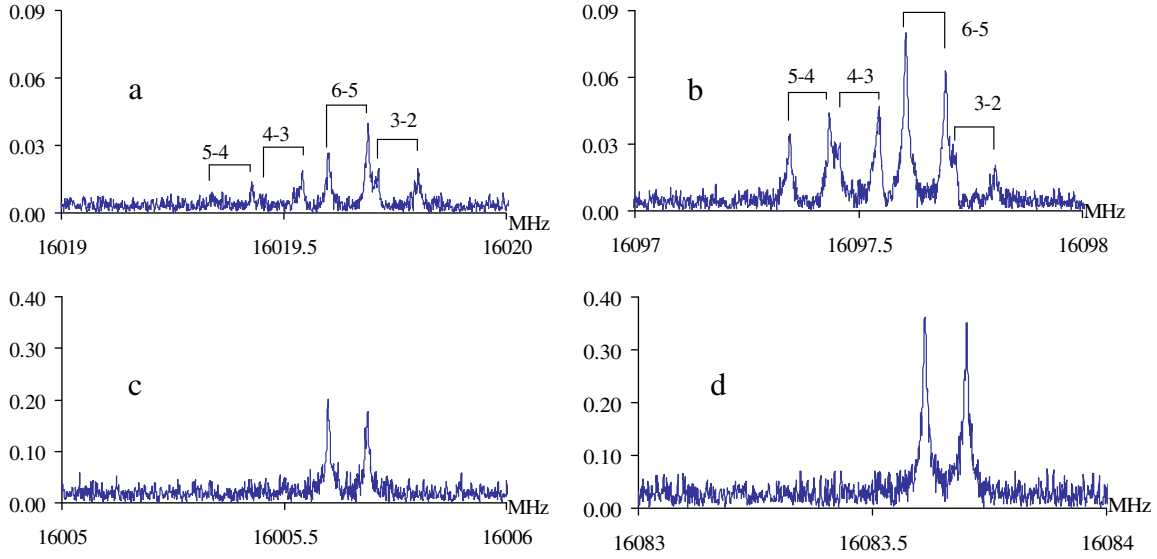

Fig. 2. The hyperfine quadrupole structure and tunneling splitting are shown for the $4_{1,3} \leftarrow 3_{0,3}$ transition: (a) and (b) DFM–^{131}Xe($0^+ \leftarrow 0^-$ and $0^- \leftarrow 0^+$), (c) and (d) DFM–^{132}Xe($0^+ \leftarrow 0^-$ and $0^- \leftarrow 0^+$).

Table 4
Dissociation energy, R_{cm} for CH_2F_2–RG, with RG = Ar, Kr, and Xe.

	DFM–Ar	DFM–Kr	DFM–Xe
R_{cm}/Å	3.35	3.616	3.816
θ/°	34.7	26.0	27.7
E_B/kJ mol^{-1}	1.5	1.9	2.1
Reference	[10]	[11]	This work

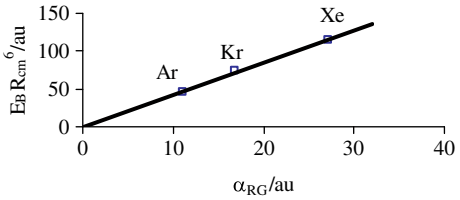

Fig. 3. $E_B\ R_{cm}^{\ 6}$ against α_{RG} gives a linear plot for the DFM–RG series.

more precise fitting. So the stretching force constant (k_s), estimated with the pseudo diatomic approximation [17]:

$$k_s = 16\pi^4\mu^2R_{cm}^2[4B^4 + 4C^4 - (B-C)^2(B+C)^2]/(hD_J) \quad (3)$$

also changed from k_s = 1.49 Nm^{-1} to k_s = 1.74 Nm^{-1}. Similarly, the dissociation energy calculated with the approximated equation $E_B = k_s R_{cm}^{\ 2}/72$, increased from 1.8 to 2.1 kJ mol^{-1}. This new value is given in Table 4 together with the values of DFM–Ar and DFM–Kr. In the Table, also the R_{cm} and θ structural parameters, useful to locate the rare gas atom, are given. Since the van der Waals interaction in DFM–RG complex is expected to be dispersively bound, the dissociation energy in these complexes should be proportional to the term $\alpha_{RG}\alpha_{DFM}/R_{cm}^{\ 6}$, where α_{RG} and α_{DFM} are the polarisabilities of the rare gas atom and of the DFM molecule, respectively. Hence, a plot of $E_B\ R_{cm}^{\ 6}$ vs. α_{RG} should be a straight line passing through the origin. This is indeed the case, after the improving of the fits with the new measurements, as shown in Fig. 3. The same linear behaviors have been observed in the series pyridine–RG series [9], CH_2ClF–RG [8] and propylene oxide–RG [18].

In conclusions, with the FTMW measurements, we could resolve the hyperfine structure of the rotational transitions of DFM–^{131}Xe, due to the quadrupole coupling of the nuclear motion of ^{131}Xe with overall rotation and tunneling motion of xenon atom. The full set of χ_{gg} (g = a, b, c) quadrupole coupling constants was obtained; the non-zero values indicate that the isotropic electron distribution of isolated ^{131}Xe is slightly distorted by its interactions with the nuclear and electronic charges of DFM molecule.

The combination of the millimeter wave [12] and FTMW measurements allowed to obtain very precise values of the centrifugal distortion constants. The dissociation energy has then been estimated from the D_J parameter, within the pseudodiatomic approximation. The dissociation energies obtained in the complexes series of DFM–RG display a linear dependence of the quantity $E_B\ R_{cm}^{\ 6}$ against α_{RG}, showing that the interaction bound between a rare gas atom and DFM is essentially a dispersive effect and the reliability of the pseudo-diatomic model formulas for van der Waals complexes.

References

[1] J.-U. Grabow, A.S. Pine, G.T. Fraser, F.J. Lovas, R.D. Suenram, T. Emilsson, E. Arunan, H.S. Gutowsky, J. Chem. Phys. 102 (1995) 1181.
[2] Y. Xu, W. Jäger, J. Djauhari, M.C.L. Gerry, J. Chem. Phys. 103 (1995) 2827.
[3] W. Jäger, Y. Xu, M.C.L. Gerry, J. Chem. Phys. 99 (1993) 919.
[4] Y. Xu, W. Jäger, M.C.L. Gerry, J. Chem. Phys. 100 (1994) 4171.
[5] Q. Wen, W. Jäger, J. Chem. Phys. 122 (2005) 214310.
[6] Q. Wen, W. Jäger, J. Phys. Chem. A 111 (2007) 2093.
[7] W. Caminati, A. Millemaggi, J.L. Alonso, A. Lesarri, J.C. Lopez, S. Mata, Chem. Phys. Lett. 392 (2004) 1.
[8] P. Ottaviani, F.M. Pesci, L.B. Favero, B. Velino, W. Caminati, Chem. Phys. Lett. 466 (2008) 122.
[9] S. Tang, L. Evangelisti, B. Velino, W. Caminati, J. Chem. Phys. 129 (2008) 144301.
[10] J.C. López, P.G. Favero, A. Dell'Erba, W. Caminati, Chem. Phys. Lett. 316 (2000) 81;
P. Ottaviani, S. Melandri, W. Caminati, J.C. López, J. Mol. Spectrosc. 239 (2006) 24.
[11] A. Maris, S. Melandri, W. Caminati, I. Rossi, Chem. Phys. Lett. 407 (2005) 192.
[12] W. Caminati, J. Phys. Chem. A. 110 (2006) 4359.
[13] T.J. Balle, W.H. Flygare, Rev. Sci. Instrum. 52 (1981) 33.
[14] J.-U. Grabow, W. Stahl, Z. Naturforsch A. 45 (1990) 1043;
J.-U. Grabow, Doctoral thesis, Christian-Albrechts-Universität zu Kiel, Kiel, 1992.;
J.-U. Grabow, W. Stahl, H. Dreizler, Rev. Sci. Instrum. 67 (1996) 4072;
J.-U. Grabow, Habilitationsschrift lllllll, Universität Hannover, Hannover, 2004. http://www.pci.uni-hannover.de/~lgpca/spectroscopy/ftmw.
[15] H.M. Pickett, J. Mol. Spectrosc. 148 (1991) 371.
[16] J.K.G. Watson, in: J.R. Durig (Ed.), Vibrational Spectra and Structure, vol. 6, Elsevier, Amsterdam, 1977, p. 1.
[17] S.E. Novick, S.J. Harris, K.C. Janda, W. Klemperer, Can. J. Phys. 53 (1975) 2007.
[18] S. Blanco, S. Melandri, A. Maris, W. Caminati, B. Velino, Z. Kisiel, PCCP 5 (2003) 1359.